Modeling of spectral changes for depth localization of fluorescent inclusion

Jenny Svensson and Stefan Andersson-Engels

Lund University Medical Laser Centre, Department of Physics, Lund Institute of Technology,
P.O. Box 118, SE-221 00 Lund, Sweden
jenny.svensson@fysik.lth.se

Abstract: We have performed modeling of fluorescence signals from inclusions inside turbid media to investigate the influence of a limited fluorescence contrast and how accurately the depth can be determined by using the spectral information. The depth was determined by forming a ratio of simulated fluorescence intensities at two wavelengths. The results show that it is important to consider the background autofluorescence in determining the depth of a fluorescent inclusion. It is also necessary to know the optical properties of the tissue to obtain the depth. A 20% error in absorption or scattering coefficients yields an error in the determined depth of approximately 2-3 mm (relative error of 10-15%) in a 20 mm thick tissue slab.

©2005 Optical Society of America

OCIS codes: (170.5280) Photon migration; (170.3660) Light propagation in tissues; (170.6510) Spectroscopy, tissue diagnostics

---

References and links

1. S. Gross and D Piwnica-Worms, "Spying on cancer: Molecular imaging in vivo with genetically encoded reporters," Cancer Cells. **7,** 5-15 (2005).
2. T. F. Massoud and S. S. Gambhir, "Molecular imaging in living subjects:seeing fundamental biological processes in a new light," Genes & Development. **17,** 545-580 (2003).
3. K Shah, A. Jacobs, X. O. Breakefield, and R. Weissleder, "Molecular imaging of gene therapy for cancer," Gene Therapy. **11,** 1175-1187 (2004).
4. V. Ntziachristos, C. Bremer, and R. Weissleder, "Fluorescence imaging with near-infrared light: new technological advances that enable in vivo molecular imaging," Eur. Radiol. **13,** 195-208 (2002).
5. C. Bremer, V. Ntziachristos, and R. Weissleder, "Optical-based molecular imaging: contrast agents and potential medical applications," Eur. Radiol. **13,** 231-243 (2003).
6. V. Ntziachristos, C.-H. Tung, C. Bremer, and R. Weissleder, "Fluorescence molecular tomography resolves protease activity *in vivo*," Nature Medicine. **8,** 757-760 (2002).
7. V. Ntziachristos, C. Bremer, E. Graves, J. Ripoll, and R. Weissleder, "In vivo tomographic imaging of near-infrared fluorescent probes," Molecular Imaging. **1,** 82-88 (2002).
8. V. Ntziachristos, E. A. Schellenberger, J. Ripoll, D. Yessayan, E. Graves, A. Bogdanov, L. Josephson, and R. Weissleder, "Visualization of antitumor treatment by means of fluorescence molecular tomography with an annexin V-Cy5.5 conjugate," Proc. Natl. Acad. Sci. USA. **101,** 12294-12299 (2004).
9. X Gao, L Yang, J. A. Petros, F. F. Marshall, J. W Simons, and S. Nie, "In vivo molecular and cellular imaging with quantum dots," Current Opinion in Biotechnology. **16,** 63-72 (2005).
10. X. Michalet, F. F. Pinaud, L. A. Bentolila, J. M. Tsay, S. Doose, J. J. Li, G. Sundaresan, A. M. Wu, S. S. Gambhir, and S. Weiss, "Quantum dots for live cells, in vivo imaging and diagnostics," Science. **307,** 538-544 (2005).
11. J. Swartling, J. Svensson, D Bengtsson, K Terike, and S. Andersson-Engels, "Fluorescence spectra provide information on the depth of fluorescent lesions in tissue," Appl. Opt. **44,** 1934-1941 (2005).
12. S. Avrillier, E. Tinet, D. Ettori, J.-M. Tualle, and B. Gélébart, "Influence of the emission-reception geometry in laser-induced fluorescence spectra from turbid media," Appl. Opt. **37,** 2781-2787 (1998).
13. M. Keijzer, R. R. Richards-Kortum, S. L. Jacques, and M. S. Feld, "Fluorescence spectroscopy of turbid media: Autofluorescence of the human aorta," Appl. Opt. **28,** 4286-4292 (1989).
14. Q. Liu and N. Ramanujam, "Experimental proof of the feasibility of using fiber-optic probe for depth-sensitve fluorescence spectroscopy of turbid media," Opt Lett. **29,** 2034-2036 (2004).
15. Q. Liu, C. Zhu, and N. Ramanujam, "Experimental validation of Monte Carlo modeling of fluorescence in tissues in the UV-visible spectrum," J. Biomed. Opt. **8,** 223-236 (2003).

---

16. M. G. Muller, I. Georgakoudi, Q. Zhang, J. Wu, and M. S. Feld, "Intrinsic fluorescence spectroscopy in turbid media: disentangling effects of scattering and absorption," Appl. Opt. **40,** 4633-4646 (2001).
17. T. J. Pfefer, L. S. Matchette, A. M. Ross, and M. N. Ediger, "Selective detection of fluorophore layers in turbid media: the role of fiber-optic probe design," Opt Lett. **28,** 120-122 (2003).
18. S. Andersson-Engels, A. Gustafson, J. Johansson, U. Stenram, K. Svanberg, and S. Svanberg, "Laser-induced fluorescence used in localizing atherosclerotic lesions," Lasers Med. Sci. **4,** 171-181 (1989).
19. T. H. Foster, E. L. Hull, M. G. Nichols, D. S. Rifkin, and N. Schwartz, "Two-steady-state methods for localizing a fluorescent inhomogeneity in a turbid medium" in *Optical Tomography and Spectroscopy of Tissue: Theory, Instrumentation, Model, and Human Studies II*, B. Chance and R. R. Alfano, eds., Proc. SPIE **2979**, 741-749 (1997).
20. E. L. Hull, M. G. Nichols, and T. H. Foster, "Localization of luminescent inhomogeneities in turbid media with spatially resolved measurements of cw diffuse luminescence emittance," Appl. Opt. **37,** 2755-2765 (1998).
21. M. S. Patterson, S. Andersson-Engels, B. C. Wilson, and E. K. Osei, "Absorption spectroscopy in tissue-simulating materials: a theoretical and experimental study of photon paths," Appl. Opt. **34,** 22-30 (1995).
22. M. S. Patterson and B. W. Pogue, "Mathematical model for time-resolved and frequency-domain fluorescence spectroscopy in biological tissues," Appl. Opt. **33,** 1963-1974 (1994).
23. J. Swartling, A. Pifferi, A. M. K. Enejder, and S. Andersson-Engels, "Accelerated Monte Carlo model to simulate fluorescence spectra from layered tissues," J. Opt. Soc. Am. A. **20,** 714-727 (2003).
24. A. Torricelli, A. Pifferi, P. Taroni, E. Giambattistelli, and R. Cubeddu, "In vivo optical characterization of human tissues from 610 to 1010 nm by time-resolved reflectance spectroscopy," Phys. Med. Biol. **46,** 2227-2237 (2001).
25. S. A. Prah,. "Optical Absorption of Hemoglobin." (Oregon Medical Laser Center, 2004), http://omlc.ogi.edu/spectra/hemoglobin/index.html
26. S. Montán, K. Svanberg, and S. Svanberg, "Multi-color imaging and contrast enhancement in cancer tumor localization using laser-induced fluorescence in hematoporphyrin derivative (HpD)-bearing tissue," Opt. Lett. **10,** 56-58 (1985).
27. K. M. Yoo, F. Liu, and R. R. Alfano, "Imaging through a scattering wall using absorption," Opt. Lett. **16,** 1068-1070 (1991).
28. T. Svensson, J. Swartling, P. Taroni, A. Torricelli, P. Lindblom, C. Ingvar, and S. Andersson-Engels. "Characterization of normal breast tissue heterogeneity using time-resolved near-infrared spectroscopy." Phys. Med. Biol. (to be published).
29. C. Eker, S. Montán, E. Jaramillo, K. Koizumi, C. Rubio, S. Andersson-Engels, K. Svanberg, S. Svanberg, and P. Slezak, "Clinical spectral characterisation of colonic mucosal lesions using autofluorescence and δ aminolevulinic acid sensitisation," Gut. **44,** 511-518 (1999).
30. N. Ramanujam, M. F. Mitchell, A. Mahadevan-Jensen, S. L. Thomsen, G. Staerkel, A. Malpica, T. Wright, N. Atkinson, and R. Richards-Kortum, "Cervical precancer detection using a multivariate statistical algorithm based on laser-induced fluorescence spectra at multiple excitation wavelengths," Photochem. Photobiol. **64,** 720-735 (1996).
31. V. V. Verkhusha and K. A. Lukyanov, "The molecular properties and applications of Anthozoa fluorescent proteins and chromoproteins," Nature Biotechnology. **22,** 289-296 (2004).
32. S. R. Arridge, "Optical tomography in medical imaging," Inverse Problems. **15**, R41-R93 (1999)

1. Introduction

One biomedical field where fluorescent inclusions are to be found is molecular imaging, where biological processes can be studied at cellular and molecular levels [1-3]. Biological processes can be monitored by using specific molecular probes, which seek out target molecules. These probes are frequently designed to provide characteristic fluorescence. To collect the induced fluorescence light, an optical imaging technique is employed.

Detection of fluorescence light emitted from the molecular probes can be used to determine the spatial location of specific cells inside the tissue and the concentration of the probe. Several optical imaging techniques can be used to detect tissue luminescence: fluorescence reflectance imaging (FRI), bioluminescence imaging (BLI) and fluorescence-mediated molecular tomography (FMT) [2-4].

One aspect of molecular imaging is the development of molecular probes emitting in the NIR region, where tissue exhibits low absorption, allowing deep penetration of light into the tissue. In the NIR region, deeply located inclusions could then also be monitored in highly vascularized tissue [5]. Molecular probes emitting fluorescence in the NIR region are desirable and under development [5-10]. Presently most fluorescence detection is conducted

with probes fluorescing in the visible, mainly by fluorescent proteins. Tissue autofluorescence is relatively high in this wavelength region, leading to a relatively low fluorescence contrast between the fluorescence from the probe at low concentrations and tissue autofluorescence [5]. Fluorescence contrast is defined as the ratio of the induced fluorescence in the fluorescent probe and the background fluorescence. Visible light also has low penetration in tissue, and deeply located inclusions, especially in tissue with a high hemoglobin concentration, are difficult to detect.

In a previous study, we demonstrated a method to determine the depth of an embedded inclusion marked with a fluorescent probe [11]. As the depth, size of inclusion, and concentration are parameters that can be difficult to evaluate independently with fluorescence imaging [4], independent information on any of these parameters will make the determination and localization of the object more accurate. The demonstrated method relies on spectral changes in the fluorescence as it propagates through the tissue. The characteristics of the detected fluorescence light depend on many different factors, for example, the optical properties of the tissue, the depth of the fluorescent inclusion, and the detection geometry [12-18]. Studies to determine the depth of a luminescent source embedded in a liquid phantom have been performed previously [19,20]. The concept of forming a ratio of acquired data to determine the depth of a fluorescent inclusion has been reported using two different excitation beam diameters [19]. An expression of diffusion theory for the emittance from a luminescent source has been fitted to spatially resolved measurements of the diffuse reflectance, providing an accuracy of the depth of an isotropic point source of 1 mm [20]. Also Patterson *et al.* used fluorescence to study the depth of light transport in tissue [21,22].

The absorption coefficient in tissue is strongly wavelength-dependent in the region from the visible to the NIR region. The dependence of tissue absorption and scattering on wavelength leads to a spectral change in the fluorescence light as it propagates through the tissue, especially the dependence of tissue absorption has been discussed in [18]. The deeper a fluorescent lesion is located in the tissue, the greater the change in intensity between different fluorescence wavelengths. In our previous study [11], the depth of a fluorescent layer was determined with both Monte Carlo simulations and experiments on a liquid phantom, by studying the fluorescence emitted in the 800–900 nm range in reflection geometry. The depth of a fluorescent layer could be determined with an accuracy of 0.6 mm down to a depth of 10 mm.

The aim of this study was to further investigate the usefulness of a depth-resolving technique based on spectral information in the visible wavelength region. Two fluorescence wavelengths (540 nm and 615 nm) were chosen where difference in tissue absorption is large. The wavelengths could in principle be chosen according to a difference in tissue scattering, but as the differences in scattering in general are smaller, the wavelengths were selected based on absorption changes. Limited fluorescence contrast and uncertainties in the optical properties are two important issues in the technique investigated here, especially of importance for detection in the visible region. The effect on a calculated ratio between the fluorescence intensities at two wavelengths as a function of depth was investigated when the optical properties were changed. Low fluorescence contrast is also a realistic problem when working in the visible wavelength region, because of the tissue autofluorescence emitted upon illumination with blue-green light. When working in the NIR region the problem with low fluorescence contrast is much smaller, because tissue autofluorescence is very weak in this wavelength region. The fluorescence contrast will be low when working with fluorescent proteins, because most of them fluoresce in the visible region.

2. Material and methods

2.1 Geometry of the modeled tissue

In Fig. 1, a schematic of the simulation geometry is shown. A layered structure is assumed. The model of tissue is divided into 60 elements in the radial direction, each element being 0.05 cm wide. The z-direction is divided into 80 or 120 elements depending on the thickness of the model, each element being 0.025 cm long. A fluorescent layer with a thickness of 1 mm can be inserted at any depth in the model.
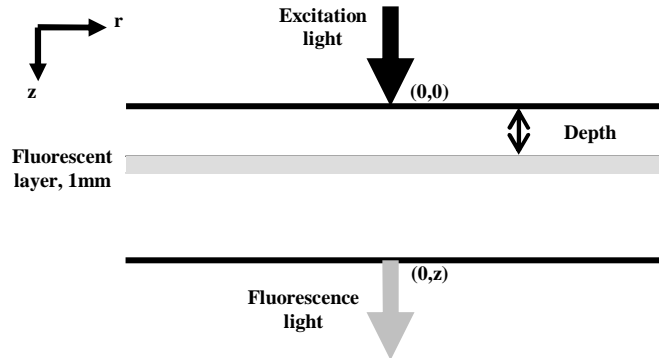

Fig. 1. Schematic of the geometry used to simulate fluorescence with Monte Carlo calculations. It assumes a layered structure, where z denotes the thickness of the sample.

A pencil beam is assumed to enter the phantom at the point $(r,z) = (0,0)$, as illustrated in Fig. 1. The transmitted fluorescence light is detected as a function of the radius, r. This corresponds to illumination with a thin laser beam and imaging detection of the transmitted fluorescence.

2.2 Fluorescence Monte Carlo simulations

An accelerated fluorescence Monte Carlo method, described in detail previously [23], was used to simulate the fluorescence generated inside an object and its transport to the back surface, where it could be detected. In this code, a Monte Carlo simulation is first performed using optical properties specified for the modeled tissue at the excitation wavelength. This simulation provides an absorption map of the fluorophore. Another simulation is then performed at the fluorescence emission wavelength, yielding a probability distribution of the generated fluorescence inside the volume to be detected at position $(0,z)$. The matrices for the excitation and emission wavelengths are then convolved to yield the probability of detecting a transmitted fluorescent photon (Γ) as a function of radial distance. Additional inputs to the Monte Carlo simulations, apart from the optical properties of the different layers and the geometry, are the fluorescence contrast and the absorption coefficient of the fluorophores in the fluorescent layer and surrounding tissue. The simulations are accelerated by using a reciprocity theorem. With this concept only one simulation is required for each emission wavelength, rather than one per wavelength for each volume element in the model [23].

2.3 Evaluation of the data

For each wavelength a vector with the probability of detecting a transmitted fluorescence photon as a function of radial distance was calculated. The ratio of the vectors obtained from simulations at two different emission wavelengths was calculated according to Eq. (1):

$$\gamma = \frac{\Gamma(540)}{\Gamma(615)} \qquad (1)$$

Data from a point (0,z) was selected for the illustrations, in order to easily compare the results of the ratio as a function of depth for different parameters in the same graph.

2.4 Optical properties of the tissue model

The optical properties used in the simulations were extracted from the results presented in Ref. [24]. In that study, the measurements were performed on *in vivo* muscle tissue with relatively low blood content. The relations in Eqs (2) and (3) were employed to obtain optical properties at the wavelengths used, where hemoglobin and oxyhemoglobin are assumed to be the dominant absorbers in the visible wavelength region [24]. The absorption is given by

$$\mu_a(\lambda) = \sum_i c_i \varepsilon_i(\lambda) \qquad (2)$$

where c_i is the concentration and ε_i is the extinction coefficient of the absorbing molecule, while the reduced scattering can be expressed as

$$\mu_s'(\lambda) = a\lambda^b \qquad (3)$$

The extinction coefficients for hemoglobin and oxyhemoglobin at 488 and 540 nm were obtained from Ref [25] and the concentrations of hemoglobin and oxyhemoglobin were obtained from Ref [24]. The optical properties obtained for the phantom at the three wavelengths are given in Table 1. The fluorescence yields were assumed to be the same at both wavelengths.

Table 1. Optical properties of the tissue model

Wavelength / nm	μ_a / cm^{-1}	μ_s' / cm^{-1}
488	0.89	18
540	2.13	16
615	0.14	14

2.5 Simulation of a 3 cm thick tissue model

The number of photons used in each simulation was 70 million, with a total thickness of the phantom of 3 cm. The optical properties used are given in Table 1. One simulation was performed for the excitation wavelength and for each of the two fluorescence emission wavelengths. The matrix obtained for the excitation light was multiplied, pixel-by-pixel, by the matrix giving the fluorescence yield. One such multiplication was performed for each depth of the fluorescence layer, yielding an excitation matrix for each depth of the layer. Finally, a convolution was performed between the excitation matrix and each of the two fluorescence matrices. The convolution was performed for each depth of the fluorescent layer. The depths of the layer in the model were: 1, 4, 7, 10, 13, 16, 19, 22, 25 and 28 mm from the excitation surface.

2.6 Changes in optical properties

The optical properties of the tissue model were altered slightly to evaluate the sensitivity of the fluorescence emission ratio, γ, to such variations. Five different simulations were performed, changing the absorption or reduced scattering coefficient at all wavelengths by ±20%. When not altered, the optical properties given in Table 1 were used. The properties

changed are listed in Table 2. The total thickness of the model was 20 mm, and the number of photons for each simulation was 10 million. In all other aspects, the simulations were identical to these described in Section 2.5.

Table 2. The optical properties used to simulate the effects of changes in optical properties on the fluorescence ratio.

	μ_a -20 %		μ_a +20 %		μ'_s -20 %		μ'_s +20 %	
λ / nm	μ_a / cm^{-1}	μ'_s / cm^{-1}	μ_a / cm^{-1}	μ'_s / cm^{-1}	μ_a / cm^{-1}	μ'_s / cm^{-1}	μ_a / cm^{-1}	μ'_s / cm^{-1}
488	0.71	18	1.07	18	0.89	14.4	0.89	21.6
540	1.7	16	2.56	16	2.13	12.8	2.13	19.2
615	0.11	14	0.17	14	0.14	11.2	0.14	16.8

Simulations were also performed to model how the ratio is affected when the relative attenuation of the two fluorescence wavelengths is changed. The absorption coefficient was varied for the fluorescence wavelength at 540 nm according to Table 3. The depths of the layer in the model were: 3, 7, 10, 13 and 19 mm from the excitation surface.

Table 3. Absorption coefficient of the tissue model with different attenuation at the fluorescence wavelengths

μ_a (540 nm) / cm^{-1}	μ_a (615 nm) / cm^{-1}	Factor
0.28	0.14	2
0.7	0.14	5
1.4	0.14	10
2.13	0.14	15

2.7 Contrast in fluorescent phantoms

In the last part of this study, the influence of fluorescence contrast in the tissue model was studied. Here we simulated the case where the bulk tissue surrounding the layer also exhibited fluorescence, and the contrast between the bulk tissue and the fluorescent layer was varied. The fluorescence contrast of the tissue model was assumed to be 1, 10, 25, 50, 100 and infinity. Fluorescence contrast of 1 corresponds to the situation of having only autofluorescence in the entire model and a contrast of infinity corresponds to fluorescence induced in the fluorescent layer only. The different values of the fluorescence contrast were chosen to study the trend of the intensity ratio as a function of depth when changing the contrast value. The investigated depths of the layer were 4, 10, 16, 19, 25 and 28 mm. Otherwise the input data in Section 2.5 were used.

3. Results

Figure 2 shows the simulated radial profiles in a logarithmic scale of fluorescence emitted from the surface of a tissue model containing a fluorescent layer at three different depths 13, 16 and 19 mm. The graph to the left shows the radial profiles for the transmitted fluorescence at 540 nm, while the graph in the middle shows the corresponding fluorescence at 615 nm. The graph to the right shows the radial profile of the ratio between 540 and 615 nm. These results are given for an ideal case with infinite fluorescence contrast where fluorescence is induced only in the thin fluorescent layer.
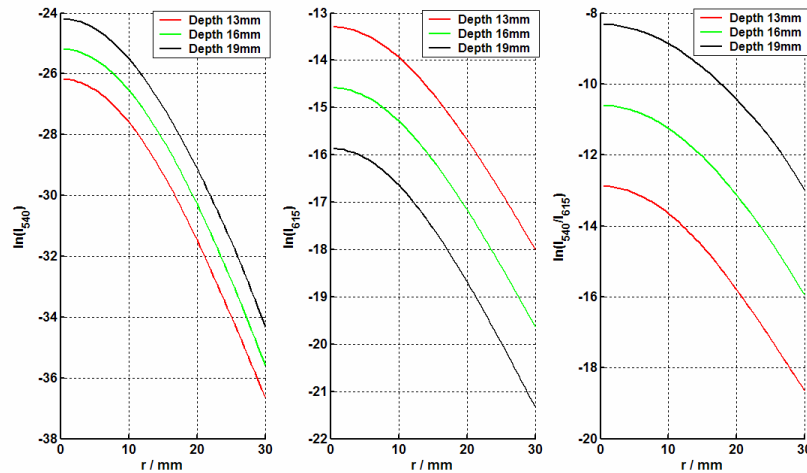
Fig. 2. Left: the radial profile for the yellow fluorescent wavelength for depths of 13, 16 and 19 mm. Middle: the radial profile for the red fluorescence at the same depths, and right: the ratio between the yellow and the red fluorescence at the same depths.

The image in the upper left corner of Fig. 3 shows the simulated distribution of the excitation light on a logarithmic scale in a tissue model, assuming the optical properties listed in Table 1 in the entire volume. The image to the lower left describes the fluorescence emitted in a layer at z = 4 mm. The images in the center show the probability of detecting fluorescence at r = 0 in the model, emitted from various positions in the model at two fluorescence wavelengths (upper row 540 nm and lower row 615 nm). These maps were modeled using a reverse Monte Carlo simulation from the backside of the model.
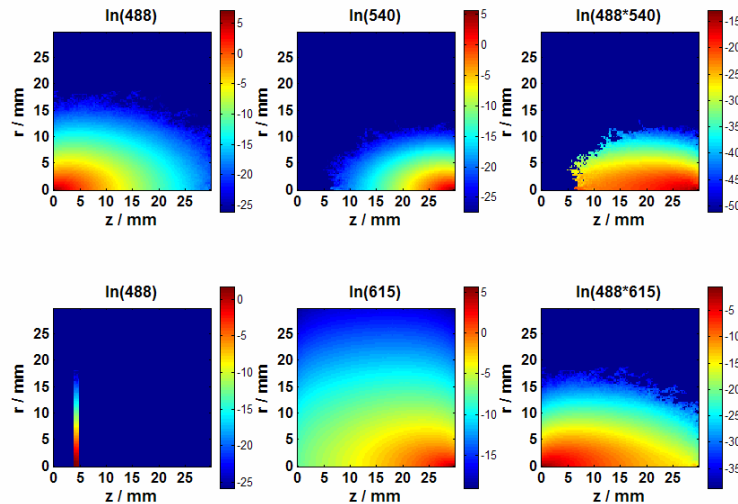

Fig. 3. Upper row: left, the distribution of the excitation light where the light can be absorbed; middle, the probability of fluorescence emitted at 540 nm to be detected at position r = 0 and z = 30; and right, the result of multiplying the excitation and emission images. Lower row: corresponding images for fluorescence emission light at 615 nm. The image in the lower left corner shows the distribution of the fluorescence emission inside the model with a fluorescence layer at z = 4 mm and an infinite fluorescence contrast.

To the right in Fig. 3, the results of a multiplication of the excitation by the fluorescence light is shown, assuming that the entire model has a uniform fluorescence efficiency of unity, i.e. using the map in the upper left corner for the excitation. This multiplication provides maps of the areas contributing to the fluorescence emitted at r = 0, and are calculated as an overlap between the excitation and the fluorescence light. Such a map is of interest when evaluating fluorescence at different wavelengths escaping the model versus the position of the fluorescent layer.

In Fig. 4 the calculated yellow/red ratio as a function of depth of the fluorescent layer is presented in logarithmic scale for various optical properties (see Table 2). The absorption or scattering coefficients for the three wavelengths were changed by ±20% at the same time. Figure 5 shows the logarithmic value of the ratio as a function of depth when the relative attenuation of the two wavelengths is changed. The absorption coefficient at 540 nm was changed to achieve a relative difference of the two wavelengths by the factors 2, 5, 10 and 15.
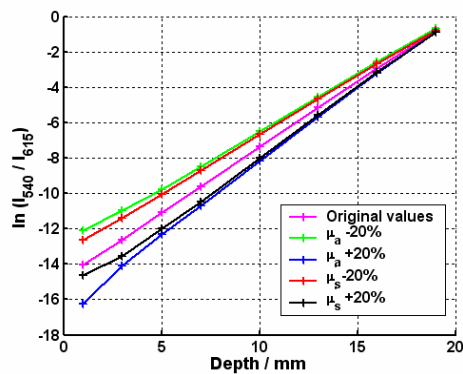

Fig. 4. Logarithmic value of the yellow/red ratio as a function of depth for optical properties according to Table 2.
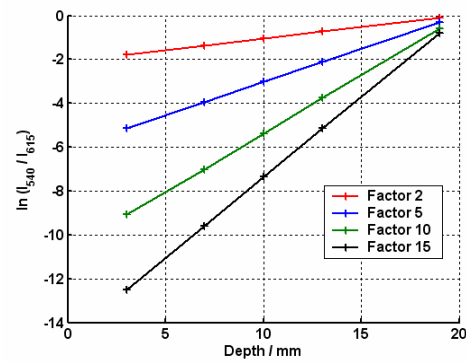
Fig. 5. Ratio of the two intensities in a logarithmic scale as a function of depth, when the relative attenuation of the two wavelengths are changed.

The results below show how the detected fluorescence is altered by autofluorescence from the surrounding bulk tissue. Figure 6 shows the detected yellow and red intensities as a function of depth of the fluorescent layer for different contrast between the layer and the rest of the tissue model and also the yellow/red ratio. As can be seen the slope of the curve decreases as the contrast is reduced, leading to a less sensitive determination of the depth of the object. For a low contrast it becomes difficult to determine the depth, especially in the center of the model.
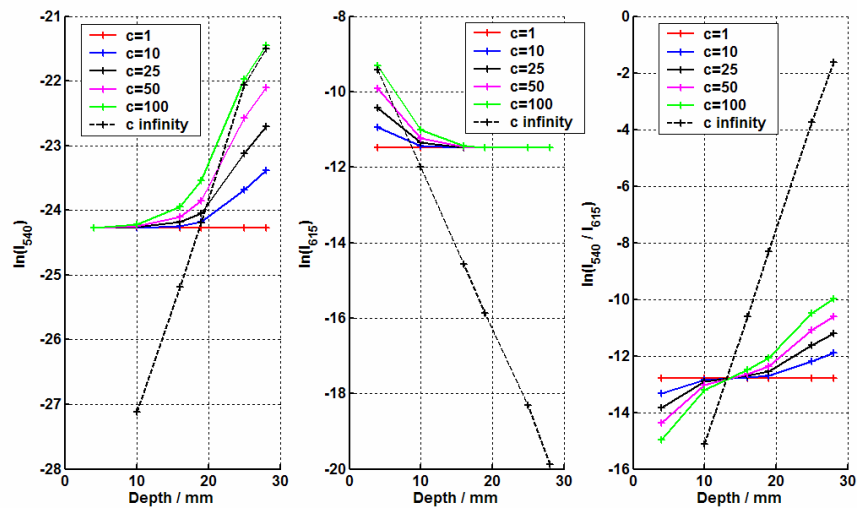
Fig. 6. Left: the detected yellow intensity as a function of the depth of the layer, middle: the corresponding for the red intensity and right: the yellow/red ratio. The legend corresponds to the contrast between the layer and the rest of the tissue model. c denotes the fluorescence contrast.

4. Discussion

Monte Carlo simulations were performed to determine the depth of a fluorescent layer inside a homogeneous tissue-like medium, assuming excitation with blue light and detection of yellow and red fluorescence wavelengths in transmission geometry. A calculated yellow/red ratio is depth-dependent when the tissue model exhibits difference in absorption at the two detection wavelengths, as the spectral shape changes as the light propagates through the medium [18].

To determine the depth, we utilized the concept of a dimensionless ratio. In real measurements there are always advantages in using a dimensionless ratio, because some of the experimental parameters will be canceled out. Examples of these parameters are fluctuations in the illumination source and object distance [26]. By forming a ratio, we limit the evaluation to two wavelengths. This automatically leads to the question of which wavelengths should be used to yield the best depth resolution and robustness. The choice of wavelengths depends on both the availability of a suitable fluorophore as well as the optical properties of the tissue and the presence of tissue autofluorescence. Below we discuss the choice of wavelength range in terms of light penetration, uncertainties in optical properties, and the presence of tissue autofluorescence.

Light obviously penetrates better, the lower the attenuation coefficient. This means that it is easier to detect fluorescence embedded in tissue in the NIR region between 600 and 900 nm, as at these wavelengths the absorption by hemoglobin, lipids and water is low. This is especially important for thick tissues containing large amounts of hemoglobin. Higher absorption will, however, preferentially attenuate light with a long path length in the tissue, yielding a less diffuse image. Increased absorption thus means a lower signal, but higher spatial resolution. This has previously been explored by Yoo *et al.* [27].

One should also choose a pair of wavelengths for which the relative attenuation is more or less independent of the exact composition of the tissue. This is of great importance when the tissue composition varies in the volume studied, or is unknown because of large interindividual variations, for example, due to lipid and water content. If two wavelengths are identified, for which different tissue types exhibit almost the same optical properties, the depth of a fluorescent inclusion can be determined much more robustly. In a previous simulation

study [11], the depth resolution for NIR fluorescence was investigated for six tissue types, ranging from water-rich to lipid-rich. Using the data obtained from those simulations, the depth of a lesion could be determined with an accuracy of 2 mm, without knowing the tissue composition. It thus seems to be possible to find such a wavelength pair around 930 nm, where water and lipids are the major absorbers, and absorb to similar degree. Variations in tissue composition are, from the absorption point of view, due to the relative amounts of lipids and water. In the visible region, where hemoglobin is the major absorber, it is not possible to find such wavelength regions, where the absorption is equal for tissue with various amount of hemoglobin. As the absorption of both wavelengths used scale linearly with the hemoglobin concentration, the relative absorption will, however, remain the same and a proper wavelength pair can thus be selected. Alterations of ±20% correspond to the variation in hemoglobin content that we found to be realistic for intersubject variation [28]. As hemoglobin is the main absorber for the excitation wavelength, as well as for both detection wavelengths in the visible region, all absorption coefficients were varied simultaneously in the simulations. The results show that a change of 20% in either the absorption or scattering coefficient still causes a considerable difference in the ratio at positions far from the detector (small depths), yielding a depth variation determined from the ratio of approximately 2–3 mm, see Fig. 4. This corresponds to a relative error in the determination of the depth of 10-15%. For layers closer to the detector the ratio is more or less independent of the optical properties, and the depth variation is only 0.5–1 mm. It is interesting to note in Fig. 4 that a change in μ_a of +20% and a change in μ_s' of +20% cause almost the same effect on the ratio. If diffusion of light can be assumed in the medium, scattering effects are described with the reduced scattering coefficient μ_s', and the remaining light fluence rate as a function of distance from a source is described by the exponential law $\exp(-\mu_{eff} \cdot d)$, where μ_{eff} is the effective attenuation coefficient, see Eq. (4), and d is the distance.

$$\mu_{eff} = \sqrt{3\mu_a(\mu_a + \mu_s')} \tag{4}$$

This explains why the change in μ_a and μ_s' provides similar results. A ±20% change in the absorption or scattering coefficient results in an approximately ±10% difference in μ_{eff}. If diffusion is assumed, the logarithmic ratio between the fluorescence intensities at two wavelengths as a function of depth will thus be linear with a slope determined by the differences in μ_{eff}. Figures 4 and 5 show linear relations of the logarithmic ratio as a function of depth, which suggests diffusion being valid. It should, however, be noted that diffusion is not always valid and non-linear shapes of the logarithmic ratio may occur.

This leads to the question of how great a difference in absorption between the two detection wavelengths is needed to achieve sufficient depth resolution. It is not always ideal to have as large difference as possible. A larger difference in absorption provides better depth resolution, but too high absorption prevents the light from penetrating deeply into the tissue. This is clearly illustrated in Fig. 3. Only inclusions close to the detector would be detected with a high absorption. Here the overlap of excitation light and emitted fluorescence light can be seen for the two fluorescence wavelengths involved. If there is no overlap, no fluorescence will be observed at the detector surface. As can be seen, no value can be obtained for the ratio for layers located at depths less than 0.5 cm when using the optical properties given in Table 1. This would be the case for the layer at the depth of 4 mm where the fluorescence would only be induced in this layer, which is indicated in the lower left image in Fig. 3. The absorption at 540 nm is so large that the light cannot reach the detector side. This can be compared to the situation when measuring in reflection geometry, then the method would be more sensitive to fluorescence from depths closer to the excitation side. These images show how important it is to select the fluorescence wavelengths carefully. If a wavelength with too high an absorption is chosen then the detectable depths will be limited to a smaller region. Another interesting remark is that the trend of the yellow fluorescence curve differs from that

of the red fluorescence curve, as can be seen in Figs. 2 and 6. The trend of the yellow fluorescence curve indicates an increase in fluorescence; this is because of the higher absorption of the yellow light compared to the absorption of the excitation light. This can also be seen in the images in the upper row in Fig. 3. For the red wavelength it is the opposite relation providing a decrease in fluorescence instead, as can also be seen in the images in the lower row in Fig. 3. In Fig. 5 it is also illustrated how important it is to know the relative attenuation of the two wavelengths used in order to determine the depth of an inclusion, as the slope of the ratio as a function of depth alters significantly with changes in the relative attenuation.

The concept of using a ratio to evaluate the spectral changes may be improved by using the statistical approach of multivariate analysis. These techniques have been used to analyze tissue in order to distinguish between malignant and non-malignant tissue and to delineate tumors in various types of tissue [29,30]. Utilizing this concept, information obtained from many wavelengths could be used to increase the depth-resolution. More spectral information should make the analysis more robust when the optical properties of the medium are not fully known. It would also reduce some of the work involved in finding the wavelength pair that provides the best depth resolution. This is something we plan to investigate in the near future.

When illuminating tissue with blue or green light, it will always emit autofluorescence. This autofluorescence is often strong compared to the weak signals from the fluorescence probe, as the volume of the surrounding tissue is so much larger than that of the embedded inclusion. Many fluorescent probes used today, for example the fluorescent proteins, emit in the visible wavelength region, where tissue autofluorescence is much stronger than in the NIR range. It is thus of importance to investigate the more realistic case when the rest of the phantom also fluoresces and not only the embedded object. The results of our Monte Carlo simulations show that a low fluorescence contrast makes it difficult to investigate the fluorescent inclusion, including determining its depth. When the fluorescence contrast is 10, the fluorescence detected from the inclusion is strongly influenced by the autofluorescence, making it difficult to determine the depth of the inclusion as illustrated in Fig. 6. It can also be seen in Fig. 6 that a tissue model containing autofluorescence only, meaning that the contrast is 1, gives a constant value of the ratio. This is a rather trivial result, as the fluorescence should be independent of the position of the layer, in this case when the layer has identical fluorescence properties as the rest of the model. The autofluorescence will contribute to a background fluorescence level. If the detectable fluorescence from the layer is not stronger than this background fluorescence, it will fall into the background noise. This is clearly shown for both wavelengths in Fig. 6. Only in the case with infinite fluorescence contrast, when the surrounding tissue has zero autofluorescence, no such effect is seen. It is interesting to note that it is in the central part of the model where it is difficult to evaluate the depth. This is due to that the 540 nm light is more absorbed than light at the excitation wavelength, yielding a positive slope of the detected fluorescence as a function of depth, while the corresponding curves for 615 nm exhibit a negative slope, as fluorescence emission at this wavelength is less attenuated than the excitation light. This yields a flat region in the central part of the model for the ratio curves. If other wavelengths with a different relation of the optical properties had been chosen, the flat region could have been at either end of the tissue model. The contribution from the autofluorescence thus clearly needs to be considered when the depth is determined by the ratio. The ongoing development of probes in the NIR region is therefore of great importance, so that imaging can be performed in the region where the tissue autofluorescence is minimized and also greater depths can be investigated. Both quantum dots and fluorescent proteins are under development in the NIR region [10,31].

In this study we focused on a homogeneous layered structure, but of course it needs to be investigated what happens for other geometries. There is also a need to study the ratio as a function of depth for a fluorescent object with a different shape. It should be noted that a large object close to the detector has the same radial profile as a small object far from the detector

[4]. It is also important to investigate how this method would work in tissues with other optical properties.

The spectral information to provide depth information of an inclusion may be shown to be useful as independent *a priori* information in tomographic evaluation algorithms. In the NIR region where scattering dominates over absorption the reconstruction of the medium becomes ill conditioned, as discussed for absorption tomography by e.g. Arridge [32]. It can thus become difficult to determine the spatial location of the object and also its size. Additional information may help to refine the reconstruction algorithm.

5. Conclusions

In this study, we have shown that the depth of a fluorescent inclusion can be determined by calculating the ratio of the intensities of two fluorescent wavelengths (yellow and red). We have especially investigated the effect on the ratio when the optical properties are changed, and with different fluorescence contrast.

Acknowledgments